

The outer kinetochore protein KNL-1 contains a defined oligomerization domain in nematodes

David M. Kern^{1,2}, Taekyung Kim³, Mike Rigney⁴, Neil Hattersley³, Arshad Desai³, and
Iain M. Cheeseman^{1,2*}

- 1 Whitehead Institute for Biomedical Research, Nine Cambridge Center, Cambridge, MA 02142
- 2 Department of Biology, MIT
- 3 Ludwig Institute for Cancer Research, Department of Cellular and Molecular Medicine, University of California at San Diego, La Jolla, California 92093, USA
- 4 Howard Hughes Medical Institute

* Corresponding author:
E-mail: icheese@wi.mit.edu
Phone: (617) 324-2503
Fax: (617) 258-5578

Characters (including spaces): 37,778

Keywords: kinetochore; centromere; mitosis; microtubule; spindle;

Running title: KNL-1 oligomerization

Abstract:

The kinetochore is a large, macromolecular assembly that is essential for connecting chromosomes to microtubules during mitosis. Despite the recent identification of multiple kinetochore components, the nature and organization of the higher order kinetochore structure remain unknown. The outer kinetochore KNL-1/Mis12 complex/Ndc80 complex (KMN) network plays a key role in generating and sensing microtubule attachments. Here, we demonstrate that *Caenorhabditis elegans* KNL-1 exists as an oligomer and we identify a specific domain in KNL-1 responsible for this activity. An N-terminal KNL-1 domain from both *C. elegans* and the related nematode *C. remanei* oligomerizes into a decameric assembly that appears roughly circular when visualized by electron microscopy. Based on sequence and mutational analysis, we

identify a small hydrophobic region as responsible for this oligomerization activity. However, mutants that precisely disrupt KNL-1 oligomerization did not alter KNL-1 localization or result in the loss of embryonic viability based on gene replacements in *C. elegans*. In *C. elegans*, KNL-1 oligomerization may coordinate with other kinetochore activities to ensure the proper organization, function, and sensory capabilities of the kinetochore-microtubule attachment.

Introduction

The kinetochore is a macromolecular protein assembly that forms the primary connection between chromosomes and spindle microtubules (Cheeseman and Desai, 2008). The major group of proteins responsible for the ability of the kinetochore to capture a microtubule is the conserved KNL-1/Mis12 complex/Ndc80 complex (KMN) network (Cheeseman *et al.*, 2004; Cheeseman *et al.*, 2006). The Ndc80 complex acts as the critical microtubule-binding element within the KMN network (Cheeseman *et al.*, 2006; DeLuca *et al.*, 2006; Wei *et al.*, 2007; Ciferri *et al.*, 2008), with the Mis12 complex acting to connect the KMN network to the inner kinetochore (Gascoigne *et al.*, 2011; Przewlaka *et al.*, 2011; Screpanti *et al.*, 2011). Finally, KNL-1 is a large protein that is required to assemble the KMN network (Cheeseman *et al.*, 2006). KNL-1 possesses a weak microtubule binding activity (Cheeseman *et al.*, 2006; Welburn *et al.*, 2010; Espeut *et al.*, 2012), and provides a scaffold for multiple signaling proteins at kinetochores including PP1 (Liu *et al.*, 2010), Bub1, and Bub3 (Kiyomitsu *et al.*, 2007; Kiyomitsu *et al.*, 2011; Krenn *et al.*, 2012; Caldas *et al.*, 2013; Vleugel *et al.*, 2013; Zhang *et al.*, 2014).

Although the protein components at the kinetochore have been largely identified, there is limited data on how these proteins assemble into a productive higher order conformation to facilitate microtubule interactions and kinetochore integrity. As prior studies have demonstrated that at least ~8-20 copies of the KMN network proteins are

bound to each microtubule at kinetochores (Joglekar *et al.*, 2006; Joglekar *et al.*, 2008; Lawrimore *et al.*, 2011), the organization of these multiple complexes is a critical task. One possibility is that the microtubule itself imparts a higher-order organization to the kinetochore elements that bind the microtubule lattice. This could occur through the intrinsic symmetry of the microtubule or simply due to spatial constraints in binding sites. Alternatively, a subset of kinetochore proteins may act to organize kinetochore proteins into the higher-order structure. For example, at centrioles, the oligomerization of the central hub element Sas6 provides the organization and 9-fold symmetry to the centriole barrel (Kitagawa *et al.*, 2011; van Breugel *et al.*, 2011). In this way, a single component of a complex could organize the remaining components to bring them into close proximity. However, it not known whether any kinetochore components self associate in a defined way that would provide such an organization to the kinetochore. Our prior work reconstituting the *C. elegans* KMN network found that KNL-1 behaved as a much larger species than would be expected based on its molecular weight (Cheeseman *et al.*, 2006). We interpreted this as a potential oligomerization for KNL-1, but the basis for and nature of this behavior was unclear.

Here, we investigated this apparent KNL-1 oligomerization activity. Our work demonstrates that nematode KNL-1 oligomerizes to a defined state at physiologically relevant concentrations. The oligomeric region forms a roughly circular structure when visualized by electron microscopy. Biochemical experiments and sequence analysis identified a small region that is conserved in nematodes as containing the oligomerization activity. However, interfering with KNL-1 oligomerization by deletion of this region or specific point mutants did not result in dramatic defects in *C. elegans* replacement experiments. We propose that nematode KNL-1 oligomerization may act in concert with other unidentified organizational elements within the kinetochore to generate a higher order kinetochore structure to organize the microtubule binding interface or signaling networks at kinetochores.

Results

The nematode KNL-1 N-terminus oligomerizes

We found previously that recombinant, full-length *C. elegans* KNL-1 behaved as a much larger species than expected based on its predicted molecular weight in size exclusion chromatography (SEC; see Fig. 1A) and sucrose gradients (Cheeseman *et al.*, 2006). We reasoned that this behavior could be due to a combination of possibilities: 1) KNL-1 aggregates non-specifically, 2) KNL-1 is highly elongated, or 3) KNL-1 oligomerizes in a structurally specific manner. To investigate the basis for this behavior, we began by creating truncations for *C. elegans* KNL-1 (see Supplemental Fig. 1A and 1B). Based on the migration of these truncations by SEC, we found that the N-terminal half of KNL-1 was sufficient to display this large apparent behavior (Fig. 1B). The N-terminus of KNL-1 acted as a single large species as revealed by both defined peaks in SEC and low polydispersity as assessed by Dynamic Light Scattering (DLS) (Fig. 1B). We further refined the region responsible for this activity to a small ~150 amino acid domain in the N-terminus of KNL-1, which we will refer to as the “oligomerization domain”. This 150 amino acid construct was well-behaved biochemically, but acted as a much larger assembly (8.6 nm Stokes radius) than expected based on its predicted molecular weight (20 kDa). For comparison, the globular thyroglobulin size standard has a similar Stokes radius of 8.5 nm, but a molecular mass of 670 kDa.

To test whether this apparent KNL-1 oligomerization activity was conserved in diverse nematode species, we analyzed the behavior of the *C. remanei* KNL-1 protein, which has diverged significantly from *C. elegans* KNL-1 (31% amino acid identity along the entire length), but displays clear homology including in the N-terminal oligomerization domain (Fig. 1C). Following purification of a recombinant *C. remanei* KNL-1 fragment with homology to the *C. elegans* oligomerization domain, we found that

the *C. remanei* protein was also oligomeric based on SEC and DLS (Fig. 1B), with the 17.6 kDa domain of *C. remanei* KNL-1 behaving as a 7.6 nm species. Thus, both *C. elegans* and *C. remanei* KNL-1 display an apparent oligomerization behavior in this conserved N-terminal region.

The KNL-1 oligomerization domain forms a defined higher-order oligomer

As both the *C. elegans* and *C. remanei* KNL-1 oligomerization domains behaved similarly as large defined species, we sought to determine whether this large size was due to specific higher-order oligomerization, or whether the protein has a highly elongated shape or is aggregation prone. To test this, we first analyzed the effect of the cross-linker glutaraldehyde on the KNL-1 oligomerization domains. At appropriate protein concentrations and time scales, glutaraldehyde will generate covalent linkages (usually between lysine residues), but only between proteins that are present in close proximity ($<7.5 \text{ \AA}$; Wine *et al.*, 2007). We found that both the *C. elegans* and *C. remanei* KNL-1 oligomerization domains could be readily cross-linked with glutaraldehyde (Fig. 2A). At high glutaraldehyde concentrations, the proteins were almost completely cross-linked into a single large species that likely corresponds to the fully cross-linked oligomer. However, at lower glutaraldehyde concentrations, we observed incompletely cross-linked species. Based on the migration of these cross-linked forms in SDS-PAGE gels, we were able to detect the presence of a ladder of incompletely cross-linked species with clear bands detected for dimers and trimers of KNL-1. Due to the apparent large size of the cross-linked domains observed by SDS-PAGE, we sought to ensure that the glutaraldehyde was not artificially generating a large oligomer through spurious interactions. To test this, we cross-linked each domain using glutaraldehyde and compared the behavior of control and cross-linked proteins by SEC (Fig. 2B). Importantly, the cross-linked KNL-1 proteins migrated similarly to the non-cross-linked proteins by SEC, and we did not observe any large cross-linked aggregates in the void

volume of the column. These crosslinking experiments demonstrate that KNL-1 subunits are in close proximity and self-associate into a higher order complex.

We next sought to determine the stoichiometry of the KNL-1 oligomer using Sedimentation Velocity Analytical Ultracentrifugation (SV-AUC). For this analysis, we observed the best fit and behavior for a larger N-terminal fragment of *C. remanei* KNL-1. The SV-AUC analysis indicated *C. remanei* KNL-1 formed a decamer, as well as having a monomeric form (Fig. 2C). Although this protein behaved primarily as a single defined species, we observed some apparent disassociation of the larger assembly during the sedimentation run based on the spread of the oligomeric peak and the fitted frictional coefficient of ~2. We also analyzed the *C. elegans* KNL-1 oligomerization domain by AUC, but we were unable to obtain a consistent fit for this protein due to a larger spread of the primary peak (data not shown), likely due to its disassociation during the assay. Based on the combination of this SV-AUC data, together with the SEC and DLS analysis, we conclude that nematode KNL-1 N-terminus forms a defined high order oligomer composed of approximately 10 subunits.

The KNL-1 oligomerization domain forms a circular structure when visualized by electron microscopy

To directly visualize KNL-1 oligomerization, we analyzed the *C. elegans* and *C. remanei* oligomerization domains by negative stain transmission electron microscopy (TEM). We found that KNL-1 was present as particles of roughly similar size and shape. Although there was some variability in individual particles, the *C. elegans* KNL-1 oligomerization domain formed a low-resolution circular or ring-like structure with a diameter of ~15 nm (Fig. 3). Similarly, the *C. remanei* oligomerization domain was present as a circular structure with a diameter of ~11 nm (Fig. 3). Thus, the KNL-1 N-terminus oligomerizes into a particle with a roughly cylindrical shape.

KNL-1 oligomerization occurs through a small hydrophobic region

We next sought to determine the structural basis and specific residues required for the oligomerization of the KNL-1 N-terminal domain. We reasoned that KNL-1 self-association could occur through hydrogen bonding, charge-charge interactions, or hydrophobic interactions. To test this, we analyzed behavior of the *C. elegans* oligomerization domain by SEC under high salt conditions (1 M NaCl). Such conditions will negate charge-charge interactions, but strengthen hydrophobic interactions. Importantly, we found that KNL-1 self-association was enhanced in 1 M NaCl (Fig. 4A), suggesting that it is dependent on hydrophobic interactions. Through sequence analysis, we identified a small region within KNL-1 that contains multiple hydrophobic residues and is conserved amongst *Caenorhabditis* species (Fig. 4C). Mutating the combination of the hydrophobic residues in this region to alanine (KNL-1 8A) abolished the oligomerization activity based on altered migration in size exclusion chromatography (Fig. 4A). Mutation of a single conserved tyrosine residue (Y137A) within this hydrophobic region strongly reduced KNL-1 oligomerization without an obvious effect on protein expression or behavior (Fig. 4A).

Furthermore, we found that when our larger N-terminal ceKNL-1 construct (aa 1-479) was tagged with superfolder GFP (sfGFP; Pedelacq *et al.*, 2006) at its C-terminus, we obtained dramatically higher protein expression compared to the untagged version (Supplemental Fig. 1C). At these high protein concentrations, we found that the KNL-1 protein formed a gel-like material after bead elution that pelleted efficiently in a centrifuge tube (Fig. 4B) and expanded the apparent bead volume during its purification (Supplemental Fig. 1C). The formation of this gel-like material as well as the observed increase in bead volume was disrupted by the KNL-1 8A mutation (Fig. 4B and Supplemental Fig. 1C). Therefore, nematode KNL-1 oligomerizes using specific residues in a small conserved hydrophobic protein region.

KNL-1 oligomerization mutants do not dramatically disrupt chromosome segregation

Based on the biochemical analyses above, nematode KNL-1 proteins undergo oligomerization. To test the contributions of this oligomerization domain to kinetochore function, we analyzed the effect of these mutants in vivo. For these experiments, we generated transgenic *C. elegans* strains using single copy *mos* insertions expressing RNAi-resistant wild type KNL-1-mCherry (see Espeut *et al.*, 2012) or mutants designed to disrupt the KNL-1 oligomerization. This includes mutations in the hydrophobic residues that are required for KNL-1 oligomerization (KNL-1 8A) or a deletion of the defined oligomerization domain (Δ 102-236). Each of these KNL-1 mutants localized to the holocentric *C. elegans* kinetochores during mitosis similar to wild type KNL-1 (Fig. 5A). To test the effects of these mutants, we depleted endogenous KNL-1 by RNAi in the transgenic strains. In the absence of transgene expression, KNL-1 depletion resulted in penetrant embryonic lethality (Fig. 5B), and eliminated kinetochore-microtubule interactions based on the rapid and premature separation of spindle poles (Fig. 5C; Desai *et al.*, 2003; Cheeseman *et al.*, 2004). Expression of wild type KNL-1-mCherry was able to fully rescue embryonic lethality (Fig. 5B) and mitotic spindle elongation behavior (Fig. 5C). Despite the significant defects in oligomerization observed in our biochemical assays, expression of the KNL-1 8A hydrophobic mutant did not result in obvious defects in embryonic lethality (Fig. 5B) or spindle pole elongation (Fig. 5C). Deletion of the entire oligomerization domain in KNL-1 (Δ 102-236) did not result in embryonic lethality (Fig. 5B), but did display a small, but reproducible delay in spindle pole elongation (Fig. 5C). We note that the Δ 102-236 deletion likely also reduces BUB-1 recruitment (Moyle *et al.*, 2014), in addition to perturbing KNL-1 oligomerization. Finally, to test whether oligomerization activity is required for the function of KNL-1 as a signaling scaffold, we generated KNL-1 mutants that disrupt both oligomerization (8A mutant) and diminish BUB-1 recruitment through mutation of the

MELT sequence repeats (Moyle *et al.*, 2014). However, the 8A+MELT double mutant displayed normal embryonic viability (Fig. 5B). Overall, these data suggest that the KNL-1 oligomerization domain is not essential. However, we speculate that this activity may synergize with other unidentified features of the nematode kinetochore to promote proper chromosome segregation.

Discussion

Our prior work suggested a potential self-association for KNL-1 (Cheeseman *et al.*, 2006). Here, we demonstrated that an N-terminal domain of nematode KNL-1 oligomerizes as a defined decameric assembly. Although this oligomerization activity is not essential for viability in *C. elegans*, it may function coordinately with additional factors to organize elements of the kinetochore. Although the oligomerization region we identified is conserved in nematode species, we did not detect obvious conservation of this domain in other organisms. We note that recent work on the human KNL1 protein has suggested the potential for its self-association through its N-terminal region based on immunoprecipitation from cells (Petrovic *et al.*, 2014). This self-interaction may indicate the binding of hKNL1 to itself, or may be mediated by one of its binding partners such as Bub1. Importantly, we note that the oligomerization that we have defined is early within the “MELT” repeat region of nematode KNL-1 (Fig. 1C), similar to the position of the Bub1-interacting “KI” motifs in human KNL1 (Kiyomitsu *et al.*, 2011). In both cases, this suggests the formation of a higher order complex of KNL1 and its spindle assembly checkpoint-binding partners at its N-terminus. Different organisms may also have distinct requirements for these features of kinetochore organization and function. For example, we note that in contrast with the human kinetochore, in *C. elegans* the Ska1 complex and the N-terminal tail of Ndc80 are dispensable for kinetochore function (Schmidt *et al.*, 2012; Cheerambathur *et al.*, 2013). It is also

possible that other kinetochore proteins may self-associate, such as has been proposed for CENP-Q (Amaro *et al.*, 2010), to contribute to kinetochore organization.

We propose that there are three principal functions for self-association of kinetochore components. First, interactions between kinetochore components may be critical for the structural integrity of kinetochores. Second, self-association of kinetochore components may be important to organize the microtubule interface. Finally, such a self-association may help to cluster signaling molecules at kinetochores. We hypothesize that the observed oligomerization for the *C. elegans* KNL-1 may play a role in organizing the N-terminus of the protein. The N-terminus of KNL-1 in all organisms is predicted to be largely disordered (Caldas and DeLuca, 2014; our unpublished analysis). Recent work has demonstrated that KNL-1 binds to Bub1 using its “MELT” repeats in this region (Krenn *et al.*, 2012; Caldas *et al.*, 2013; Vleugel *et al.*, 2013; Zhang *et al.*, 2014). As multiple repeats are present throughout the N-terminus of KNL-1, this may allow a single molecule of KNL-1 to recruit multiple Bub1 proteins (Vleugel *et al.*, 2013). Self-association of KNL-1 would act to further locally concentrate Bub1, potentially amplifying this signal for its roles in the spindle assembly checkpoint and recruiting Aurora B to centromeres. Generating a focus of signaling activity may be especially important in a holocentric kinetochore since a diffuse kinetochore poses different signaling requirements compared to a localized kinetochore. It is likely that other kinetochore components possess properties or behaviors that promote kinetochore structure and organization in parallel to KNL-1.

Materials and Methods

Plasmids

6xHis *E. coli* expression constructs for the KNL-1 oligomerization domains (His-ceKNL-1 amino acids 69-235, His-crKNL-1 amino acids 76-216, and His-crKNL-1 amino acids 76-396) were amplified from *C. elegans* cDNA or synthesized by Genewiz and cloned

into pRSETa to add an N-terminal His-tag (MRGSHHHHHHGMAS-). The 6xHis-ceKNL-1 1-479 expression constructs was generated using a modified pET3aTr vector to add a PreScission cleavable, N-terminal His-tag (MRGSHHHHHHGMASMTGGQQMGRDLYDDDDKLEVLFGQGP-). SuperfolderGFP constructs were cloned with a custom C-terminal superfolderGFP-His tag. Mutations for ceKNL-1 constructs were introduced using PCR.

Protein Production and Purification

Proteins were produced using 3-12 L of BL21 (DE3) *E. coli*. Generally, bacteria was grown to OD 0.6-1 at 30°C in LB media containing antibiotic and 0.4% glucose. The temperature was reduced to 18°C and protein production was induced with 100 mM IPTG. The bacteria was harvested 6 hours post-induction (20 hours for GFP constructs) with Lysis Buffer (50 mM Sodium Phosphate pH 8, 300 mM NaCl, 40 mM Imidazole) and frozen at -80°C. The bacterial pellet was then thawed and lysed using 1 mg/mL lysozyme and sonication. 10 mM Beta-mercaptoethanol was then added. The lysate was pelleted at 40,000 x g for 30 minutes. The supernatant was bound to Ni-NTA resin (Qiagen) for 1 hour at 4°C. The resin was washed with Wash Buffer (50 mM Sodium Phosphate pH 8, 500 mM NaCl, 40 mM Imidazole, 10 mM BME, 0.1% Tween-20). Bound protein was then eluted with Elution Buffer (50 mM Sodium Phosphate pH 7, 500 mM NaCl, 250 mM Imidazole, 10 mM BME). Elutions were loaded onto Superose 6 or Superdex 200 columns for gel filtration into Schwartz Buffer (20 mM Sodium Phosphate pH 7, 150 mM NaCl, 1 mM DTT). Peak fractions were checked using SDS-PAGE gels stained with Coomassie. The peak fractions were then pooled and spin concentrated (Vivaspin; GE Healthcare). Protein concentrations were determined using the Biorad Assay kit. Protein was used fresh (within a few days on ice and never freeze/thawed) for all experiments.

Gel Filtration

Proteins were loaded at indicated concentrations onto either a Sephacryl S-500 HR 16/60 column or a Superose 6 10/30 GL column equilibrated in Schwartz Buffer. Size standards run with matching loading volumes are marked as indicated in figures. Runs were analyzed using representative fractions spanning the column runs with SDS-PAGE gels stained with Coomassie. Note: Due to the low absorption coefficient at 280 nm for the KNL-1 protein fragments we used large Coomassie-stained gels, instead of UV traces, for visualization.

Dynamic Light Scattering

Measurements were taken using a Protein Solutions Dynapro instrument and Dynamics V6 software. The measurements were taken using 10 reads each with a 10 second averaging time.

Glutaraldehyde cross-linking

Proteins were cross-linked at the indicated concentrations of protein. Glutaraldehyde (70% stock solution, EM grade, Sigma-Aldrich) was diluted in ddH₂O to 0.2% or 1% (1% was also used for Superose 6 runs) and mixed with protein at 1:20 to the indicated final concentrations. Mock cross-linking was performed using the equivalent volume of ddH₂O. The proteins were cross-linked for 10 minutes at room temperature and then quenched with 1:10 volume of 1M Tris pH 8. For Figure 2A, the protein was loaded onto a 12% SDS-PAGE gel for visualization with Coomassie. For Figure 2B, following the quenching, the proteins were pelleted at 18,000 g and then loaded onto the Superose 6 gel filtration column in Schwartz Buffer and runs were visualized using 12% SDS-PAGE gels stained with Coomassie.

Analytical Ultracentrifugation

The sedimentation-velocity (SV) experiment for the His-crKNL-1 76-396 construct was conducted using purified protein at ~20 μ M in Schwartz Buffer using a Beckman Optima XL-I analytical ultracentrifuge in interference mode (MIT Biophysical Instrumentation Facility, MIT-BIF). Data was collected at 20°C at 25,000 rpm. The data was fit using SEDFIT to a model for continuous sedimentation coefficient distribution, assuming a single frictional coefficient. The molecular weights were estimated using the best-fit frictional coefficients.

Electron Microscopy

To prevent disassembly of the oligomers under the conditions used for EM, His-ceKNL-1 69-235 and His-crKNL-1 76-216 were cross-linked at ~5 μ M and ~10 μ M respectively using a final concentration of 0.1% Glutaraldehyde. Following quenching, protein was dialyzed into EM Buffer (20 mM Tris pH 7.5, 150 mM NaCl, 1 mM DTT) for 5 hours at 4°C. Samples were then kept on ice until grid preparation. For grid preparation, 4 μ l samples were applied to freshly glow-discharged continuous carbon grids and stained with 0.75% uranyl formate. Images were collected on an FEI Tecnai F-20 electron microscope with a Gatan US4000 CCD detector using a nominal magnification of 62,000x (83,701x at detector) and a -3 μ m defocus.

Sequence Analysis

Sequences were aligned using ClustalX and Jalview software.

Worm strains

The worm strains used in this study are listed in Table S1. The KNL-1 mutations were engineered into a vector expressing KNL-1::mCherry (Espeut *et al.*, 2012). Plasmids were injected into strain EG4322 to obtain stable single-copy integrants (Frokjaer-

Jensen *et al.*, 2008). Integration of transgenes was confirmed by PCR. For live imaging, transgenes were crossed into a strain expressing GFP::H2b/GFP:: γ -tubulin and the transgene as well as both markers were homozygosed prior to analysis.

RNA-mediated Interference

Double-stranded RNAs used in this study are listed in Table S2. All RNAi was performed by microinjection. L4 worms were injected with dsRNAs and incubated for 38–43 h at 20°C before imaging of the embryos. For lethality assays, L4 worms were injected with dsRNA and singled onto plates at 24 hours post-injection; adult worms were removed from the plates at 48 hours post-injection and hatched larvae and unhatched embryos were counted at 72 hours post-injection.

Time-lapse microscopy

For imaging of chromosomes and pole tracking analysis, images were acquired on a deconvolution microscope (DeltaVision; Applied Precision) equipped with a charge-coupled device camera (CoolSnap; Roper Scientific) with 5 x 2 μ m z-stacks, 2x2 binning, and a 60x 1.3 NA U-planApo objective (Olympus) at 10 sec intervals and 100 ms exposure at 18°C. Spindle pole separation was quantified as described (Desai *et al.*, 2003).

For KNL-1 localization, embryos expressing GFP::H2b/GFP:: γ -tubulin/KNL-1::mCherry were filmed every 20 sec with 5 x 2 μ m z-stacks on an Andor Revolution XD Confocal System (Andor Technology) and a confocal scanner unit (CSU-10; Yokogawa) mounted on an inverted microscope (TE2000-E; Nikon) equipped with 100x, 1.4 NA Plan Apochromat lens and outfitted with an electron multiplication back-thinned charge-coupled device camera (iXon, Andor Technology, binning 1x1) at 20°C. Exposure was 100 ms for GFP and 300 ms for mCherry.

Acknowledgements

Debby Pheasant and the Biophysical Instrumentation Facility for the Study of Complex Macromolecular Systems (NSF-007031) are gratefully acknowledged. We thank Nikolaus Grigorieff, Mathijs Vleugel, Bob Sauer, Thomas Schwartz, Ellen Kloss, and members of the Cheeseman laboratory for their support, input, and helpful discussions. This work was supported by a Scholar award to IMC from the Leukemia & Lymphoma Society, grants from the NIH/National Institute of General Medical Sciences to IMC (GM088313), AD (GM074215), and a Research Scholar Grant to IC (121776) from the American Cancer Society. M.R. was supported by funding from HHMI to Nikolaus Grigorieff.

References

- Amaro, A.C., Samora, C.P., Holtackers, R., Wang, E., Kingston, I.J., Alonso, M., Lampson, M., McAnish, A.D., and Meraldi, P. (2010). Molecular control of kinetochore-microtubule dynamics and chromosome oscillations. *Nat Cell Biol* 12, 319-329.
- Caldas, G.V., and DeLuca, J.G. (2014). KNL1: bringing order to the kinetochore. *Chromosoma* 123, 169-181.
- Caldas, G.V., DeLuca, K.F., and DeLuca, J.G. (2013). KNL1 facilitates phosphorylation of outer kinetochore proteins by promoting Aurora B kinase activity. *J Cell Biol* 203, 957-969.
- Cheerambathur, D.K., Gassmann, R., Cook, B., Oegema, K., and Desai, A. (2013). Crosstalk between microtubule attachment complexes ensures accurate chromosome segregation. *Science* 342, 1239-1242.
- Cheeseman, I.M., Chappie, J.S., Wilson-Kubalek, E.M., and Desai, A. (2006). The Conserved KMN Network Constitutes the Core Microtubule-Binding Site of the Kinetochore. *Cell* 127, 983-997.
- Cheeseman, I.M., and Desai, A. (2008). Molecular Architecture of the Kinetochore-Microtubule Interface. *Nat Rev Mol Cell Biol* 9, 33-46.
- Cheeseman, I.M., Niessen, S., Anderson, S., Hyndman, F., Yates, J.R., III, Oegema, K., and Desai, A. (2004). A conserved protein network controls assembly of the outer kinetochore and its ability to sustain tension. *Genes Dev.* 18, 2255-2268.
- Ciferri, C., Pasqualato, S., Screpanti, E., Varetto, G., Santaguida, S., Dos Reis, G., Maiolica, A., Polka, J., De Luca, J.G., De Wulf, P., Salek, M., Rappsilber, J., Moores, C.A., Salmon, E.D., and Musacchio, A. (2008). Implications for kinetochore-microtubule attachment from the structure of an engineered Ndc80 complex. *Cell* 133, 427-439.

- DeLuca, J.G., Gall, W.E., Ciferri, C., Cimini, D., Musacchio, A., and Salmon, E.D. (2006). Kinetochore Microtubule Dynamics and Attachment Stability Are Regulated by Hec1. *Cell* 127, 969-982.
- Desai, A., Rybina, S., Muller-Reichert, T., Shevchenko, A., Shevchenko, A., Hyman, A., and Oegema, K. (2003). KNL-1 directs assembly of the microtubule-binding interface of the kinetochore in *C. elegans*. *Genes Dev.* 17, 2421-2435.
- Espeut, J., Cheerambathur, D.K., Krenning, L., Oegema, K., and Desai, A. (2012). Microtubule binding by KNL-1 contributes to spindle checkpoint silencing at the kinetochore. *J Cell Biol* 196, 469-482.
- Frokjaer-Jensen, C., Davis, M.W., Hopkins, C.E., Newman, B.J., Thummel, J.M., Olesen, S.P., Grunnet, M., and Jorgensen, E.M. (2008). Single-copy insertion of transgenes in *Caenorhabditis elegans*. *Nat Genet* 40, 1375-1383.
- Gascoigne, K.E., Takeuchi, K., Suzuki, A., Hori, T., Fukagawa, T., and Cheeseman, I.M. (2011). Induced ectopic kinetochore assembly bypasses the requirement for CENP-A nucleosomes. *Cell* 145, 410-422.
- Joglekar, A.P., Bouck, D., Finley, K., Liu, X., Wan, Y., Berman, J., He, X., Salmon, E.D., and Bloom, K.S. (2008). Molecular architecture of the kinetochore-microtubule attachment site is conserved between point and regional centromeres. *J Cell Biol* 181, 587-594.
- Joglekar, A.P., Bouck, D.C., Molk, J.N., Bloom, K.S., and Salmon, E.D. (2006). Molecular architecture of a kinetochore-microtubule attachment site. *Nat Cell Biol* 8, 581-585.
- Kitagawa, D., Vakonakis, I., Olieric, N., Hilbert, M., Keller, D., Olieric, V., Bortfeld, M., Erat, M.C., Fluckiger, I., Gonczy, P., and Steinmetz, M.O. (2011). Structural basis of the 9-fold symmetry of centrioles. *Cell* 144, 364-375.
- Kiyomitsu, T., Murakami, H., and Yanagida, M. (2011). Protein interaction domain mapping of human kinetochore protein Blinkin reveals a consensus motif for binding of spindle assembly checkpoint proteins Bub1 and BubR1. *Mol Cell Biol* 31, 998-1011.
- Kiyomitsu, T., Obuse, C., and Yanagida, M. (2007). Human Blinkin/AF15q14 Is Required for Chromosome Alignment and the Mitotic Checkpoint through Direct Interaction with Bub1 and BubR1. *Dev Cell* 13, 663-676.
- Krenn, V., Wehenkel, A., Li, X., Santaguida, S., and Musacchio, A. (2012). Structural analysis reveals features of the spindle checkpoint kinase Bub1-kinetochore subunit Knl1 interaction. *J Cell Biol* 196, 451-467.
- Lawrimore, J., Bloom, K.S., and Salmon, E.D. (2011). Point centromeres contain more than a single centromere-specific Cse4 (CENP-A) nucleosome. *J Cell Biol* 195, 573-582.
- Liu, D., Vleugel, M., Backer, C.B., Hori, T., Fukagawa, T., Cheeseman, I.M., and Lampson, M.A. (2010). Regulated targeting of protein phosphatase 1 to the outer kinetochore by KNL1 opposes Aurora B kinase. *J Cell Biol* 188, 809-820.
- Moyle, M.W., Kim, T., Hattersley, N., Espeut, J., Cheerambathur, D.K., Oegema, K., and Desai, A. (2014). A Bub1-Mad1 interaction targets the Mad1-Mad2 complex to unattached kinetochores to initiate the spindle checkpoint. *J Cell Biol* 204, 647-657.

- Pedelacq, J.D., Cabantous, S., Tran, T., Terwilliger, T.C., and Waldo, G.S. (2006). Engineering and characterization of a superfolder green fluorescent protein. *Nat Biotechnol* 24, 79-88.
- Petrovic, A., Mosalaganti, S., Keller, J., Mattiuzzo, M., Overlack, K., Krenn, V., De Antoni, A., Wohlgemuth, S., Cecatiello, V., Pasqualato, S., Raunser, S., and Musacchio, A. (2014). Modular assembly of RWD domains on the Mis12 complex underlies outer kinetochore organization. *Mol Cell* 53, 591-605.
- Przewlaka, M.R., Venkei, Z., Bolanos-Garcia, V.M., Debski, J., Dadlez, M., and Glover, D.M. (2011). CENP-C is a structural platform for kinetochore assembly. *Current biology : CB* 21, 399-405.
- Schmidt, J.C., Arthanari, H., Boeszoermenyi, A., Dashkevich, N.M., Wilson-Kubalek, E.M., Monnier, N., Markus, M., Oberer, M., Milligan, R.A., Bathe, M., Wagner, G., Grishchuk, E.L., and Cheeseman, I.M. (2012). The kinetochore-bound Ska1 complex tracks depolymerizing microtubules and binds to curved protofilaments. *Dev Cell* 23, 968-980.
- Screpanti, E., De Antoni, A., Alushin, G.M., Petrovic, A., Melis, T., Nogales, E., and Musacchio, A. (2011). Direct binding of Cenp-C to the Mis12 complex joins the inner and outer kinetochore. *Current biology : CB* 21, 391-398.
- van Breugel, M., Hirono, M., Andreeva, A., Yanagisawa, H.A., Yamaguchi, S., Nakazawa, Y., Morgner, N., Petrovich, M., Ebong, I.O., Robinson, C.V., Johnson, C.M., Veprintsev, D., and Zuber, B. (2011). Structures of SAS-6 suggest its organization in centrioles. *Science* 331, 1196-1199.
- Vleugel, M., Tromer, E., Omerzu, M., Groenewold, V., Nijenhuis, W., Snel, B., and Kops, G.J. (2013). Arrayed BUB recruitment modules in the kinetochore scaffold KNL1 promote accurate chromosome segregation. *J Cell Biol* 203, 943-955.
- Wei, R.R., Al-Bassam, J., and Harrison, S.C. (2007). The Ndc80/HEC1 complex is a contact point for kinetochore-microtubule attachment. *Nat Struct Mol Biol* 14, 54-59.
- Welburn, J.P., Vleugel, M., Liu, D., Yates, J.R., 3rd, Lampson, M.A., Fukagawa, T., and Cheeseman, I.M. (2010). Aurora B phosphorylates spatially distinct targets to differentially regulate the kinetochore-microtubule interface. *Mol Cell* 38, 383-392.
- Wine, Y., Cohen-Hadar, N., Freeman, A., and Frolov, F. (2007). Elucidation of the mechanism and end products of glutaraldehyde crosslinking reaction by X-ray structure analysis. *Biotechnology and bioengineering* 98, 711-718.
- Zhang, G., Lischetti, T., and Nilsson, J. (2014). A minimal number of MELT repeats supports all the functions of KNL1 in chromosome segregation. *J Cell Sci* 127, 871-884.

column, with the relative elution volumes indicated. The predicted molecular weights, and the stokes radii and % polydispersity measured by Dynamic Light Scattering are indicated to the right. (C) Top, diagram showing a schematic of the *C. elegans* KNL-1 protein, with the previously defined motifs and regions indicated. Bottom, sequence alignment of the *C. elegans* and *C. remanei* oligomerization domains with conserved residues indicated and “MELT” repeats indicated with boxes.

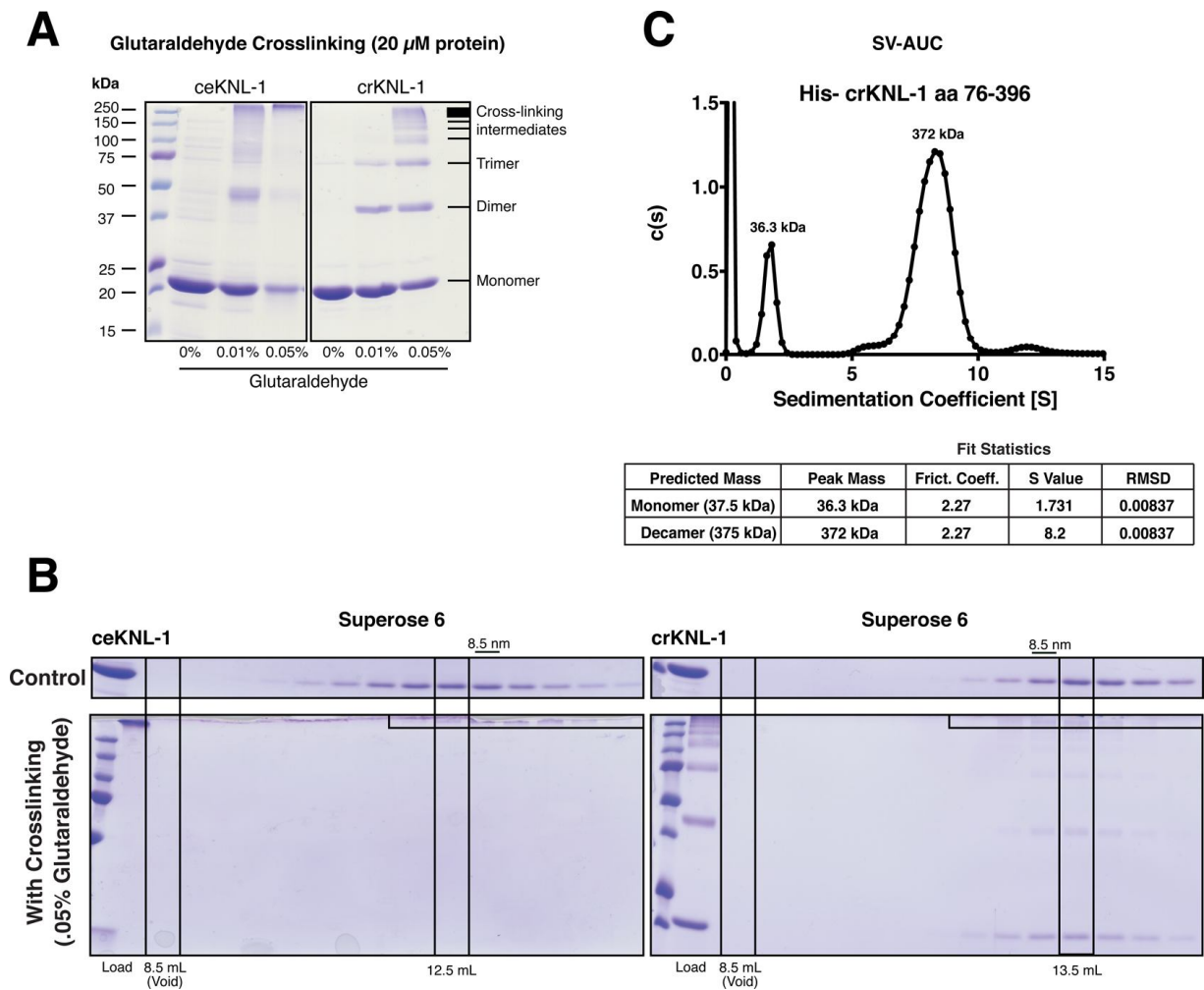
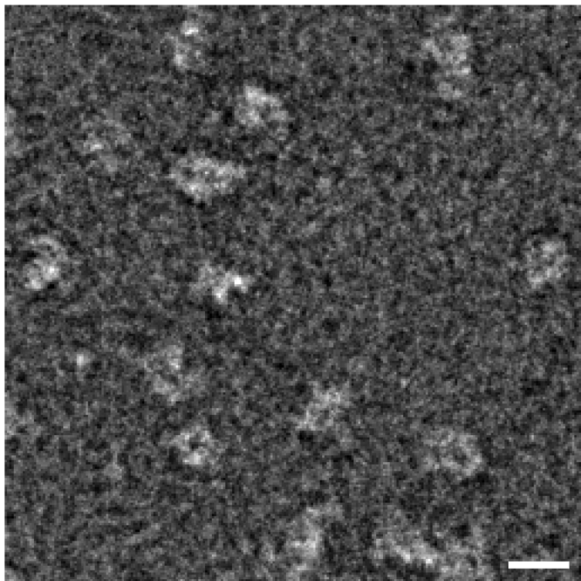
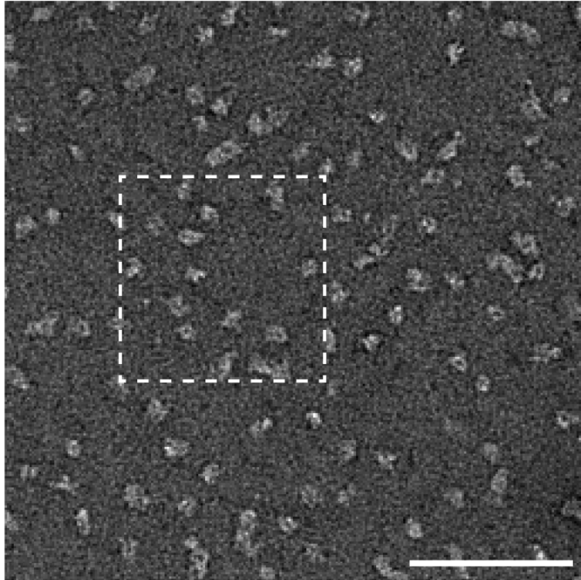


Figure 2. The KNL-1 N-terminal domain oligomerizes into a decameric assembly. (A) Coomassie-stained SDS-PAGE gels showing the *C. elegans* and *C. remanei* KNL-1 oligomerization domains (at a concentration of 20 μ M) treated with the indicated concentrations of the crosslinking agent glutaraldehyde. The shift in migration SDS-PAGE gel reflects the formation of multimeric crosslinked assemblies, as indicated on the right. (B) Coomassie-stained SDS-PAGE gels showing fractions from the size exclusion chromatography analysis of the *C. elegans* and *C. remanei* oligomerization domains. The native oligomerization domains (top) and the domains crosslinked using .05% glutaraldehyde (bottom) display similar migration indicating that this treatment does not result in protein aggregation. We note that cross-linking appears to make the oligomers slightly smaller, potentially from stabilizing disordered regions of protein. The fully crosslinked *C. elegans* protein migrates just below the stacking gel. (C) Trace from the SV-AUC analysis of *C. remanei* KNL-1 aa 76-396. Fitting of the migration behavior (bottom) is consistent with the presence of a monomeric and decameric form.

A His-ceKNL-1 aa 69-235



B His-crKNL-1 aa 76-216

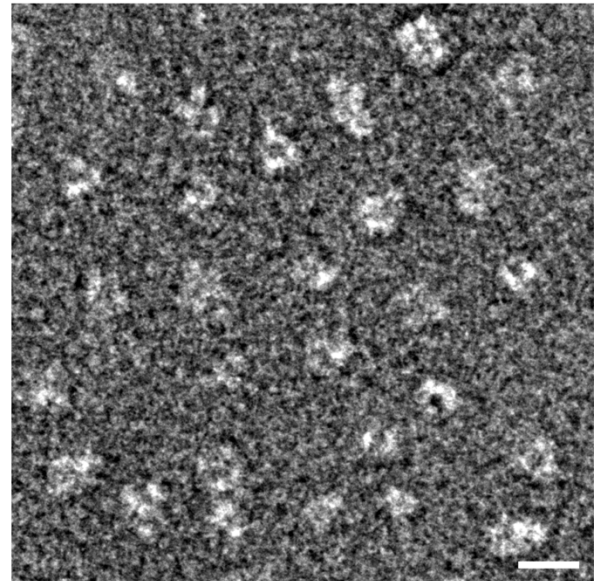
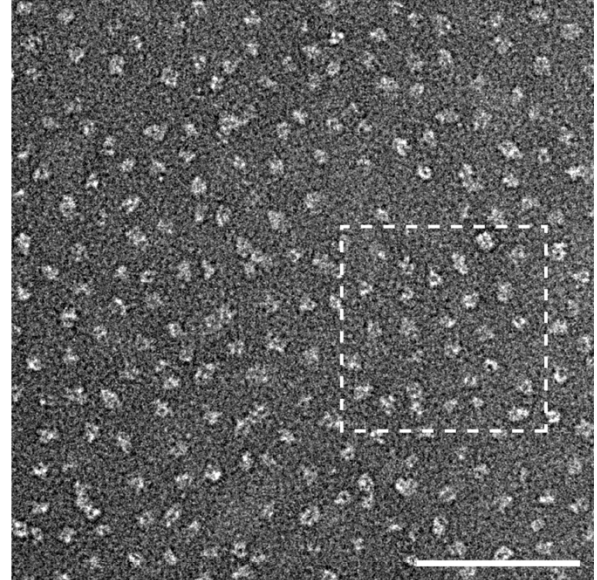
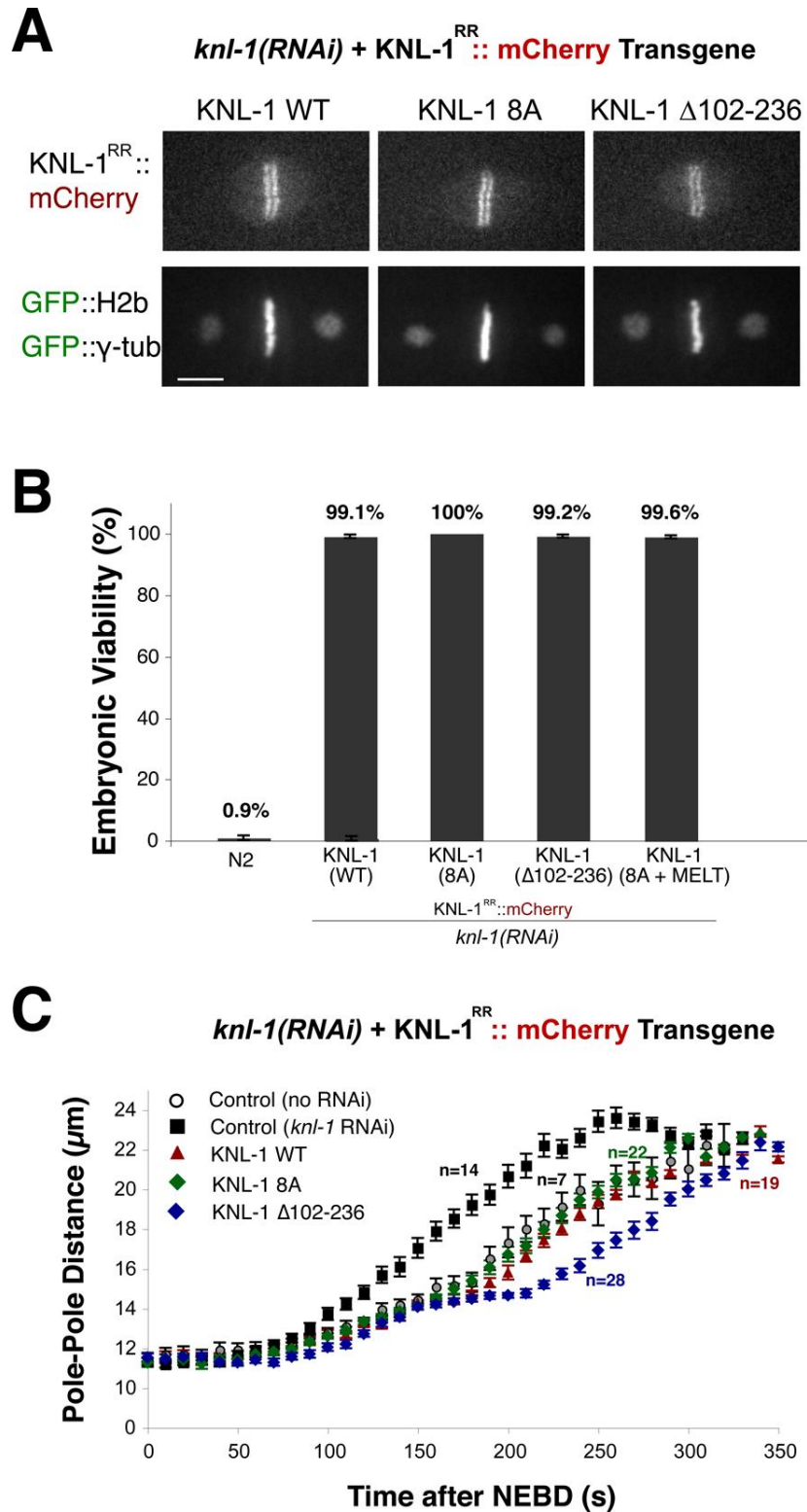


Figure 3. Visualization of the KNL-1 oligomerization domain by transmission electron microscopy. (A) Top, a field of ceKNL-1 oligomerization domain particles detected using transmsion electron microscopy with negative staining. Scale bar, 100 nm. Bottom, a zoomed-in view from the boxed region above. Scale bar, 20 nm. (B) Top, a field of crKNL-1 oligomerization domain particles. Scale bar, 100 nm. Bottom, zoomed-in view from the boxed region above. Scale bar, 20 nm.

increasing concentrations, or in the presence of 1 M NaCl as indicated. Top, migration behavior of the wild type oligomerization domain. Middle, migration behavior of the Y137A mutant, which severely compromises the oligomerization activity. Bottom, migration behavior of the 8A mutant construct (concentration is approximate due to the presence of a contaminating protein). (B) Pellets from the wild-type and 8A mutant superfolder GFP tagged proteins. The wild-type protein produces a substantial amount of a protein gel substance after nickel bead elution. This gel can be pelleted at low speed (22,000 g, not shown) and high speed (100,000 g, shown here). (C) Alignment of *Caenorhabditis* KNL-1 proteins showing the conservation of the residues in the oligomerization domain, highlighting the presence of a hydrophobic patch and the presence of the conserved tryptophan residue. Mutations included in the 8A mutant are indicated by A's above the residues.



or the indicated mutants) expressed in the first cell division *C. elegans* embryo. The bar-like localization reflects localization to the holocentric *C. elegans* kinetochores. Scale bar, 5 μ m. (B) Graph indicating the embryonic viability following KNL-1 RNAi for N2 worms (n = 7 worms and 1512 embryos), or worms stably expressing wild type KNL-1 (n = 7 worms and 733 embryos), KNL-1 8A (n = 10 worms and 1041 embryos), KNL-1 Δ 102-236 (n = 6 worms and 676 embryos), and KNL-1 8A + MELT (n = 13 worms and 1269 embryos). The graph shows the percent viability \pm standard error. (C) Graph showing spindle pole separation over time during the first embryonic cell division for control embryos (Control (no RNAi); n = 7), or KNL-1 RNAi embryos (Control (KNL-1 RNAi); n = 14), or KNL-1 RNAi embryos expressing KNL-1 wild type (n = 19), KNL-1 8A (n = 22), or KNL-1 Δ 102-236 (n = 28). Error bars represent standard error. The curves are aligned with respect to nuclear envelope breakdown (NEBD).